

The Solar Twin Planet Search: The age - chromospheric activity relation [★]

Diego Lorenzo-Oliveira¹, Fabrício C. Freitas¹, Jorge Meléndez¹, Megan Bedell^{2,7}, Iván Ramírez³, Jacob L. Bean², Martin Asplund⁴, Lorenzo Spina^{1,8}, Stefan Dreizler⁵, Alan Alves-Brito⁶, and Luca Casagrande⁴

¹ Universidade de São Paulo, Departamento de Astronomia do IAG/USP, Rua do Matão 1226, Cidade Universitária, 05508-900 São Paulo, SP, Brazil. e-mail: diegolorenzo@usp.br

² University of Chicago, Department of Astronomy and Astrophysics, USA

³ Tacoma Community College, 6501 South 19th Street, Tacoma, Washington 98466, USA

⁴ The Australian National University, Research School of Astronomy and Astrophysics, Cotter Road, Weston, ACT 2611, Australia

⁵ Institut für Astrophysik, Universität Göttingen, Germany

⁶ Instituto de Física, Universidade Federal do Rio Grande do Sul, Porto Alegre, Brazil

⁷ Center for Computational Astrophysics, Flatiron Institute, 162 5th Ave., New York, NY 10010, USA

⁸ Monash Centre for Astrophysics, School of Physics and Astronomy, Monash University, VIC 3800, Australia

June 22, 2018

ABSTRACT

Context. It is well known that the magnetic activity of solar type stars decreases with age, but it is widely debated in the literature whether there is a smooth decline or if there is an early sharp drop until 1-2 Gyr followed by a relatively inactive constant phase.

Aims. We revisited the activity-age relation using time-series observations of a large sample of solar twins whose precise isochronal ages and other important physical parameters have been determined.

Methods. We measured the Ca II H and K activity indices using ≈ 9000 HARPS spectra of 82 solar twins. In addition, the average solar activity was calculated through asteroids and Moon reflection spectra using the same instrumentation. Thus, we transformed our activity indices into the S Mount Wilson scale (S_{MW}), recalibrated the MW absolute flux and photospheric correction equations as a function of T_{eff} , and then computed an improved bolometric flux normalized activity index $\log R'_{\text{HK}}(T_{\text{eff}})$ for the entire sample.

Results. New relations between activity and age of solar twins were derived assessing the chromospheric age-dating limits using $\log R'_{\text{HK}}(T_{\text{eff}})$. We measured an average solar activity of $S_{MW} = 0.1712 \pm 0.0017$ during solar magnetic cycles 23–24 covered by HARPS observations and we also inferred an average of $S_{MW} = 0.1694 \pm 0.0025$ for cycles 10–24, anchored on a S index vs. sunspot number correlation. Also, a simple relation between the average and dispersion of the activity levels of solar twins was found. This enabled us to predict the stellar variability effects on the age-activity diagram and, consequently, estimate the chromospheric age uncertainties due to the same phenomena. The age-activity relation is still statistically significant up to ages around 6–7 Gyr, in agreement with previous works using open clusters and field stars with precise ages.

Conclusions. Our research confirms that Ca II H& K lines remain a useful chromospheric evolution tracer until stars reach ages of at least 6–7 Gyr. We found an evidence that, for the most homogenous set of old stars, the chromospheric activity indices seem to continue decreasing after the solar age towards the end of the main-sequence. Our results indicate that a significant part of the scatter observed in the age-activity relation of solar twins can be attributed to stellar cycle modulations effects. The Sun seems to have a normal activity level and variability for its age.

Key words. stars: solar-type – stars: evolution – stars: fundamental parameters – magnetic fields

1. Introduction

The solar-type stars' chromospheric activity is one of the observed manifestations of a broad phenomenon called stellar magnetic activity, which is expected to be driven by the same physical principles of the Solar dynamo. The paradigm is that the complex interplay between turbulent convection and rotation triggers the stellar cyclic and self-sustained global magnetic ac-

tivity (Parker 1970). As the star ages, it is expected that its rotation and, consequently, magnetic activity, decreases due to angular momentum loss through magnetized winds and structural variations along evolutionary timescales.

Therefore, considering this theoretical framework, rotation (Skumanich 1972; Barnes 2007; Barnes & Kim 2010; Reiners & Mohanty 2012; dos Santos et al. 2016) and magnetic activity (Skumanich 1972; Soderblom et al. 1991; Mamajek & Hillenbrand 2008; Lorenzo-Oliveira et al. 2016b) are frequently considered as interesting clocks optimized for main-sequence solar-type mass stars. Alternatively, some authors estimate stellar ages using classical techniques such as isochrones (e.g., Ng & Bertelli 1998; Lachaume et al. 1999; Ramírez et al. 2014; Nissen 2015), and the use of chemical abundance markers such as the Li abundance (e.g., Skumanich 1972; Do Nascimento et al. 2009; Carlos et al. 2016) or, more recently, the [Y/Mg] or [Y/Al] ratio (e.g.,

[★] Based on observations collected at the European Organisation for Astronomical Research in the Southern Hemisphere under ESO programs 188.C-0265, 183.D-0729, 292.C-5004, 097.C-0571, 092.C-0721, 093.C-0409, 072.C-0488, 183.C-0972, 091.C-0936, 192.C-0852, 196.C-1006, 076.C-0155, 096.C-0499, 185.D-0056, 192.C-0224, 075.C-0332, 090.C-0421, 091.C-0034, 077.C-0364, 089.C-0415, 60.A-9036, 092.C-0832, 295.C-5035, 295.C-5031, 60.A-9700, 289.D-5015, 096.C-0210, 086.C-0284, 088.C-0323, 0100.D-0444, and 099.C-0491.

Nissen 2015; Tucci Maia et al. 2016; Spina et al. 2016b,a). A review of different methods to estimate stellar ages is given by Soderblom (2010), who also discussed the problems affecting the different age indicators.

The first parametrization of the activity-age relation was performed by Skumanich (1972), where the chromospheric emission of the Ca II H & K lines was used as activity indicator. While there are other important magnetic activity tracers such as high-energy coronal emissions (Ribas et al. 2005; Booth et al. 2017), Mg II h & k (Oranje & Zwaan 1985; Buccino & Mauas 2008), H α (Pasquini & Pallavicini 1991; Lyra & Porto de Mello 2005), H β (Montes et al. 2001), Ca II infrared triplet (Busà et al. 2007; Lorenzo-Oliveira et al. 2016a), the Ca II H & K lines are widely used because they are readily measurable from ground-based observatories, and also there is a consistent and ready-to-use absolute flux calibration available in the literature.

Most of the previous works suggested a smooth decrease of chromospheric activity with increasing age (Soderblom et al. 1991; Mamajek & Hillenbrand 2008; Lorenzo-Oliveira et al. 2016b), but Pace & Pasquini (2004) and Pace (2013) suggested that activity-age relations are only valid for stars younger than approximately 1.5 Gyr, with no further decay in activity after this age. The authors analysed high-resolution UVES observations of 35 FG-type members of 5 open clusters spanning a wide age interval from Hyades to M67, and the Sun, resulting in a fit between chromospheric flux or $v \sin i$, and age. In addition, Pace (2013) assessed the age-activity diagram also through hundreds of FGK dwarfs with photometric effective temperatures and metallicities from Casagrande et al. (2011), and open clusters, to indicate a plateau after ~ 1.5 Gyr. This result, combining a heterogeneous sample of field stars and open clusters is an independent confirmation of previous findings of Lyra & Porto de Mello (2005) using the H α line, and is also in line with Pace & Pasquini (2004).

On the other hand, recent work by Lorenzo-Oliveira et al. (2016b) using dozens of M67 (≈ 4 Gyr) and NGC 188 (≈ 6 Gyr) G dwarfs observed with Gemini North GMOS shows that the activity evolution could be extended until at least 6 Gyr. Furthermore, the authors point out that the lack of activity evolution after 1.5 Gyr could be interpreted as a mass/effective temperature and metallicity bias that affects Ca II H & K fluxes, in addition to isochronal age sample selection bias.

Therefore, the most convenient way to rule out the effects of other variables on Ca II activity levels (Rutten & Schrijver 1987; Rocha-Pinto & Maciel 1998; Gray et al. 2006; Lovis et al. 2011; Lorenzo-Oliveira et al. 2016a), minimizing biases in the age-activity correlation, is the study of chromospheric activity evolution of open clusters members (Soderblom et al. 1991; Mamajek & Hillenbrand 2008), wide binaries (Garcés et al. 2011; Desidera et al. 2006), or field stellar twins with similar mass and metallicity. In this work we adopted the last option, reassessing the age-chromospheric activity relation using a large sample of solar twins (Ramírez et al. 2014). These stars are very similar to the Sun, since their stellar parameters (T_{eff} , $\log g$, [Fe/H]) are roughly within ± 100 K, ± 0.1 dex, ± 0.1 dex of the Sun's values¹. As the stars have very similar physical properties (mass and metallicity), the main parameter affecting changes in stellar activity is their ages. In a broader context, the magnetic activity history of our Sun is important for planetary habitability (Ribas et al. 2005; Airapetian & Usmanov 2016; do Nascimento et al. 2016) and to constrain dynamo models (e.g., Karak et al. 2014; Pipin & Kosovichev 2016).

This paper is organised as follows: Sec. 2 describes our working sample and the procedures adopted to build a new Ca II H & K chromospheric activity index. We also investigate the solar activity variability in comparison to the solar twins. In Sec. 3 we describe the derivation of isochronal ages for the entire sample and revisit the age-activity relation. The discussion of our results is presented in Sec. 4. The summary and conclusions are drawn in Sect. 5.

2. Data, measurement and calibration

2.1. Working Sample

Our sample was selected from the 88 solar twins presented in Ramírez et al. (2014). From this sample, we obtained data for 70 stars with the HARPS instrument (Mayor et al. 2003) at the 3.6 m telescope at the La Silla observatory, to search for planets around solar twins (program 188.C-0265, Bedell et al. 2015; Meléndez et al. 2015, 2017). Additional data for 12 stars were found in the ESO archive, as detailed in Table 1. Thanks to the high quality and cadence time-series observations, combined with the excellent instrumental stability of the HARPS spectrograph, it is possible to explore the limits of chromospheric ageing using Ca II lines.

To measure the solar activity index we used spectra from Ceres, Europa, Vesta, and the Moon (ESO projects 60.A-9036, 60.A-9700, 086.C-0284, 088.C-0323, 092.C-0832, 096.C-0210, 289.D-5015, 295.C-5031, and 295.C-5035) and correlate with the International Sunspot Number from WDC-SILSO (version 2.0), Royal Observatory of Belgium, Brussels.²

2.2. Contamination of spectroscopic binaries

We have visual and spectroscopic binaries in our sample, as marked in Table 2. Spectroscopic binaries may have a different evolution from the other stars because, in principle, the interaction with its partner can change the angular momentum and consequently the chromospheric activity, so they were ignored in the age-activity analysis. We cross-matched our sample with the subsample of spectroscopic binaries analysed by dos Santos et al. (2017), Tucci Maia et al. (2016) and Fuhrmann et al. (2017). In addition, we removed the remaining stars with companions within $4''$, accordingly to these studies. In total, 21 stars fell in these selection criteria: HIP6407, HIP14501, HIP18844, HIP19911, HIP30037, HIP54102, HIP54582, HIP62039, HIP64150, HIP64673, HIP65708, HIP67620, HIP72043, HIP73241, HIP79578, HIP81746, HIP83276, HIP87769, HIP103983, HIP109110, and HIP116906. Some of the spectroscopic binaries show enhanced rotation velocities for their ages (dos Santos et al. 2016, 2017). Illustrating a few cases, HIP67620 has also been identified as anomalously high in [Y/Mg] (Tucci Maia et al. 2016), being evidence of mass transfer from a former AGB companion, causing a rejuvenation in stellar activity due to transfer of angular momentum. This star is probably a solar twin blue straggler, like HIP10725 (Schirbel et al. 2015). The stars HIP19911 also has enhanced Y abundances for its age (Tucci Maia et al. 2016), suggesting a link to the blue straggler phenomenon.

¹ $T_{\text{eff}}^{\odot} = 5777\text{K}$, $\log g^{\odot} = 4.437$, as adopted in Ramírez et al. (2014).

² <http://www.sidc.be/silso>

2.3. Calibration to the Mount Wilson System

The Ca II H and K activity indices were calculated from HARPS spectra following Mount Wilson (MW) prescriptions presented in Wright et al. (2004). We compared our S_{HARPS} index for the entire sample of solar twins against their respective S_{MW} found in the literature (Duncan et al. 1991; Henry et al. 1996; Wright et al. 2004; Meléndez et al. 2009; Jenkins et al. 2011; Ramírez et al. 2014). In order to provide a more reliable calibration, a subsample of solar twins with the lowest S_{MW} uncertainties ($\sigma \leq 0.012$) were selected, excluding the Sun. From this subsample, our S index measurements were converted into the MW system, resulting in the following transformation equation:

$$S_{\text{MW}} = 0.9444 S_{\text{HARPS}} + 0.0475, \quad (1)$$

where S_{HARPS} is defined as:

$$S_{\text{HARPS}} = 18.349 \frac{H + K}{R + V}. \quad (2)$$

The typical standard deviation for the most inactive stars is 0.004 ($S_{\text{MW}} \leq 0.190$) and 0.014 for the active ones ($S_{\text{MW}} > 0.190$). For each sample star, we provide in Table 1 its S_{MW} collected from the literature as well as their respective ESO project identifications. The average values and standard deviation of the S values, already calibrated to the Mount Wilson system using the Eq. 1, are given in Table 2.

We tested the possibility of S_{MW} offsets between the observations performed before and after the HARPS June 2015 upgrade (Lo Curto et al. 2015). Considering our S_{MW} calibration uncertainties, our results based on 46 stars indicate that both epochs are statistically similar, since the median S_{MW} absolute deviation is 0.003, which turns out to be only $\sim 1\%$ of their S values.

2.4. An improved activity scale for $\log(R'_{\text{HK}})$ indices

From the S index we made the conversion to R_{HK} , which is the total flux (F) in units of $\text{erg cm}^{-2}\text{s}^{-1}$ at the stellar surface in the H and K lines normalized by the bolometric flux ($F_{\text{HK}}/\sigma T_{\text{eff}}^4$). However R_{HK} has a strong photospheric contamination (R_{phot}) that needs to be properly corrected in order to pull out the chromospheric signature of the Ca II H & K lines (R'_{HK}). Thus, as a first step, we strictly followed the prescriptions from Wright et al. (2004) that calibrate the activity measurements as a function of (B-V) color indices and S_{MW} :

$$R_{\text{HK}} = 1.34 \times 10^{-4} C_{\text{cf}} S_{\text{MW}}, \quad (3)$$

where

$$\log C_{\text{cf}}(B - V) = 1.13(B - V)^3 - 3.91(B - V)^2 + 2.84(B - V) - 0.47. \quad (4)$$

The C_{cf} term is proportional to the bolometric normalized absolute continuum flux in the R and V Mount Wilson passbands, and the photospheric correction as a function of (B-V) is given by:

$$\log R_{\text{phot}}(B - V) = -4.898 + 1.918(B - V)^2 - 2.893(B - V)^3. \quad (5)$$

Finally, we obtained our activity indices R'_{HK} through Eqs. 3-4, and then subtracting Eq. 3 by Eq. 5:

$$R'_{\text{HK}} = R_{\text{HK}} - R_{\text{phot}}. \quad (6)$$

The applicability of these equations are limited to late-F up to early K dwarfs. Recently, Suárez Mascareño et al. (2015, 2016) extended the validity of C_{cf} and R_{phot} calibrations towards the M dwarf regime ($0.4 \lesssim (B - V) \lesssim 1.9$).

In order to test the consistency of our activity measurements, we cross-matched our sample with those of Lovis et al. (2011) and found 14 solar-twins in common. The mean difference in $\log R'_{\text{HK}}(B - V)$ between both databases (Lovis-Ours) is $\Delta \log R'_{\text{HK}}(B - V) = +0.006 \pm 0.033$ dex. The (B-V) colors were taken mostly from the solar twin catalogue of UBV photometry by Ramírez et al. (2012b) and complemented with other values from the literature, as explained in Ramírez et al. (2014). We did not correct for redenning because most of our sample are located within a volume around the centre of a dust-free cavity (Lallement et al. 2014). The only exception is HIP114615 ($d=103^{+22}_{-15}$ pc) which is at a high galactic latitude ($b=-68^\circ$), having thus a negligible extinction, $E(B-V)=0.020$ according to Schlegel et al. (1998), and 0.017 according to the correction by Schlafly & Finkbeiner (2011) or 0.008 adopting the correction proposed by Meléndez et al. (2006).

The equations 4 and 5 have the disadvantage of using the (B-V) color to calculate the photospheric and chromospheric contributions of Ca II H & K lines, but these are directly related to T_{eff} and [Fe/H] rather than (B-V) (Rocha-Pinto & Maciel 1998; Lovis et al. 2011; Lorenzo-Oliveira et al. 2016b). So, in order to minimize these degeneracies, we recalibrated the MW system by replacing the (B-V) for T_{eff} . To do so, we cross-matched the 72 stars of Noyes et al. (1984) with those of Ramírez et al. (2013). This subsample covers a wide range of T_{eff} , from 4350 K up to 6500 K. Thus, we investigated a new relation between R_{phot} (Noyes et al. 1984, Table 1) and T_{eff} (Ramírez et al. 2013) (plotted in Fig. 1):

$$\log R_{\text{phot}}(T_{\text{eff}}) = -4.78845 - \frac{3.70700}{1 + (T_{\text{eff}}/4598.92)^{17.5272}}. \quad (7)$$

After that, we calibrated the C_{cf} as a function of T_{eff} using the values found in Rutten (1984), excluding the giant stars. In total, 52 stars in the original Rutten (1984) sample were cross-matched with those from Ramírez et al. (2012a, 2013). The calibration follows below (plotted in Fig. 1):

$$\log C_{\text{cf}}(T_{\text{eff}}) = (-1.70 \times 10^{-7}) T_{\text{eff}}^2 + (2.25 \times 10^{-3}) T_{\text{eff}} - 7.31. \quad (8)$$

Fig 2 shows that both approaches are strongly correlated to each other. The only significant difference appears as we consider progressively more inactive stars, where the classical MW activity indices seem to decrease their sensitivity to small activity variations, as evidenced by our new approach. Therefore, we expect that the $\log R'_{\text{HK}}(T_{\text{eff}})$ should be a better indicator of activity evolution of most inactive and old stars. Probably, the use of B-V color collapses the effective temperature and metallicity effects which might give more direct information about the absolute continuum flux distribution (see, e.g., Lorenzo-Oliveira et al. 2016a). This effect is more evident in inactive stars where the chromospheric/photospheric contrast is weaker.

2.5. The activity variability of the Sun and solar twins

It has been shown by Bertello et al. (2016) that the disk integrated Ca II index has a strong linear correlation with sunspot number, although the Ca II line fluxes are expected to be better correlated to solar plages. In any case, solar plages and the presence of sunspots are different manifestations of the same underlying phenomena (namely magnetic activity) and, therefore,

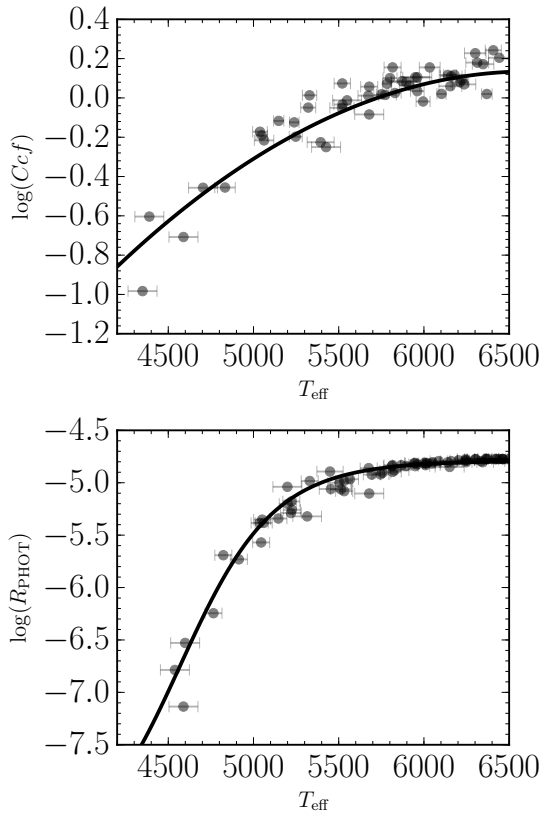


Fig. 1. Upper panel: The C_{cf} of the stars cited in Rutten (1984). The black line represents our fit described in Eq. 8. Lower panel: The $\log R_{\text{phot}}$ of the stars from Noyes et al. (1984). The black line represents our fit described in Eq. 7.

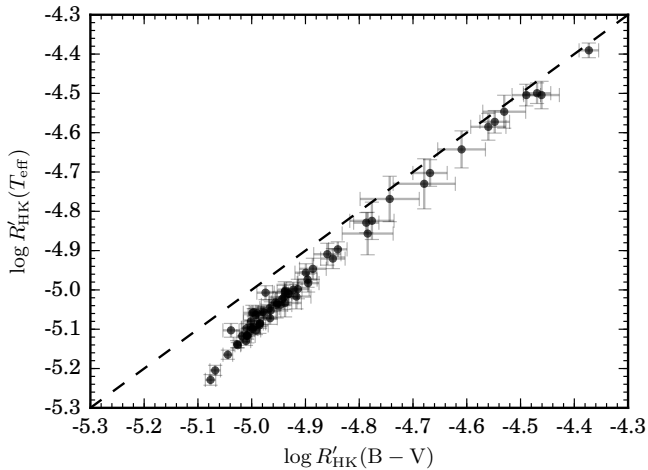


Fig. 2. The $\log(R'_{\text{HK}})$ using (B-V) vs. the $\log(R'_{\text{HK}})$ using the T_{eff} . The errorbars represent the intrinsic dispersion of the multiple observations. The black traced line represents the 1:1 relation.

they should be somewhat related to each other. Thus we could perform a calibration between the S-index and sunspot number, allowing us to increase our time baseline, for obtaining a more accurate average S-index. For each day that the S-index was measured we related it with the mean between the number of sunspots one day earlier and one day after the observation, using the WDC-SILSO sunspot numbers. In Fig. 3, we show the correlation between our S_{MW} and sunspot number. The sunspot

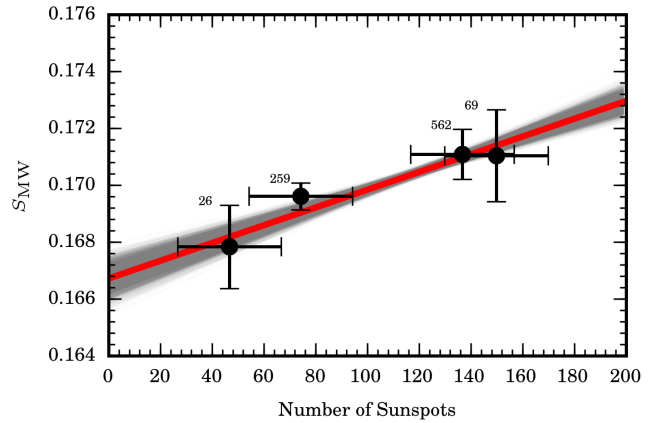


Fig. 3. The measured S index against the International Sunspot Number (WDC-SILSO) around the same day. The red line represents the best fit between them, as presented in Eq. 9. The gray lines are the Bisector regression fitting of 10^5 Monte Carlo simulations based on the activity dispersion in each sunspot number bin. The numbers placed on the top of each error bar represent the number observations that were considered to estimate its mean and dispersion.

number and the activity measurements were binned into 4 intervals of 40 sunspots each with their respective average (in activity and sunspot number) and dispersion represented by the error bars. Through 10^5 Monte Carlo simulations, assuming gaussian error distribution, we derived a mean relation between the solar activity and sunspot number, followed by its respective uncertainties:

$$S_{\text{MW}} = (3.12 \pm 0.28) \times 10^{-5} N + (0.1667 \pm 0.0003), \quad (9)$$

where N is the International Sunspot Number defined by the Royal Observatory of Belgium. The internal error of this approach is $\sigma_{S_{\text{MW}}} = 0.00038 \pm 0.00009$. This relation allowed us to estimate the solar activity level along the cycles 10-24 (1856–2017, see Fig. 4). We found $\langle S_{\text{MW}} \rangle (10-24) = 0.1694 \pm 0.0024$ (± 0.0004 , from Eq. 9). To check the consistency of our reconstructed solar activity history, we restricted our predictions to cycles 15–24, also analysed by Egeland et al. (2017) who found $\langle S_{\text{MW}} \rangle (15-24) = 0.1694 \pm 0.0020$. Our result of $\langle S_{\text{MW}} \rangle (15-24) = 0.1696 \pm 0.0025$ indicates a similar mean activity level and dispersion along these cycles, confirming the overall consistency of our approach. Also, we averaged the cycles 23-24 activity measurements from HARPS observations of the Moon and the other solar-system bodies (Ceres, Vesta, and Europa, hereafter SSB). The differences between them were negligible ($\langle S_{\text{MW}} \rangle^{\text{Moon}} = 0.1714 \pm 0.0011$ and $\langle S_{\text{MW}} \rangle^{\text{SSB}} = 0.1706 \pm 0.0027$) so we combined all available spectra in order to obtain a more consistent measurement of the solar activity level ($\langle S_{\text{MW}} \rangle^{\text{SSB+Moon}} = 0.1712 \pm 0.0017$). This result derived from HARPS spectra is also in agreement with our predictions for $\langle S_{\text{MW}} \rangle (10-24)$. For an extensive discussion about S_{MW} determinations and calibration issues among different authors and instruments see Egeland et al. (2017); in this context our results for the Sun are accurate, as its measurements were made with the same instrumentation as for the stars calibrated into the MW scale.

In Fig 5, a few illustrative cases of stellar chromospheric variability as a function of age are shown. According to our data, the amplitude of activity variations tends to decrease towards older and inactive stars. Interestingly, the well-known solar twin HIP79672 (Porto de Mello & da Silva 1997; Meléndez et al.

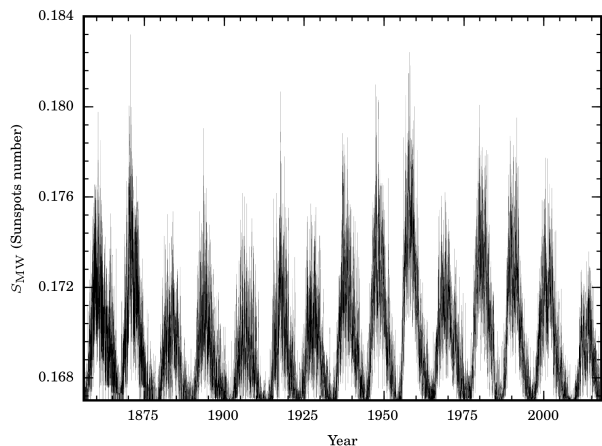


Fig. 4. The daily solar S index (using the eq. 9) since 1850. Solar chromospheric cycles 10–24 reconstructed from the relation between S_{MW} vs. Number of sunspots (see Fig. 3).

2014, red circles) shows cycle modulation and amplitude that resembles the Sun (gray shaded region).

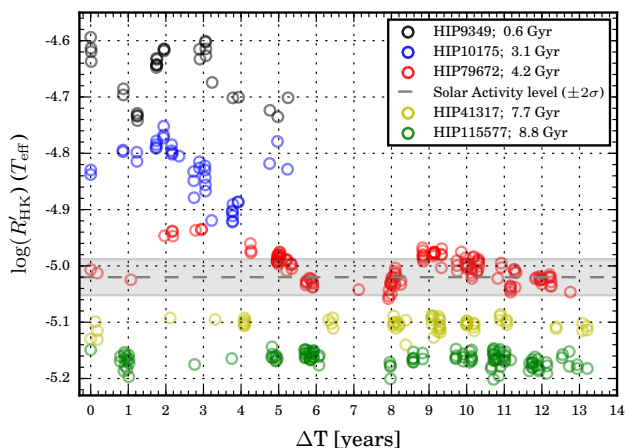


Fig. 5. Solar twins activity modulations over the years of observations. The gray dashed line and filled area correspond to the mean Sun's $\log R'_{HK}(T_{\text{eff}})$ level and its fluctuations within $\pm 2\sigma$, respectively. Each circle is the nightly averaged level of activity, for multiple observations.

It is well known that the amplitude of cycle modulations of cool stars is roughly related to its activity levels (Baliunas et al. 1995; Suárez Mascareño et al. 2015, 2016; Egeland et al. 2017) which, for instance, should depend on its evolutionary state (Reiners & Mohanty 2012; Schröder et al. 2013; Mittag et al. 2016). In this sense, we found in our sample that the standard deviation of $\log(R'_{HK})$ ($\sigma_{\log(R'_{HK})}$, possibly a proxy of the activity cycle amplitude) due to long-term variations increases towards active stars (Fig. 6). In order to have a more reliable estimate of $\sigma_{\log(R'_{HK})}$, it is important to monitor the whole activity cycle, however this is likely not the case for most of our sample stars. Thus, we stress that in some cases our derived $\sigma_{\log(R'_{HK})}$ can only represent a lower limit of the realistic R'_{HK} variation during the course of the activity cycles. Even though, we are continuously monitoring the cycle modulations of these solar twins

over the years and, in the future, we expect to provide a more robust estimate of $\sigma_{\log(R'_{HK})}$ as a function of different activity levels.

In Fig. 6 we separated our stars in three different groups: 1) Young solar twins with ages lower than 2 Gyr were assigned as green stars; 2) Middle-aged solar twins (4.5 ± 2.0 Gyr, red triangles); 3) Old solar twins with ages greater than 6.5 Gyr (black circles). Stars with time-series observations shorter than 5 years were not considered in order to minimize the effect of short-cycle variations. In the solid black line, we show the linear regression relating mean activity levels $\log R'_{HK}(T_{\text{eff}})$ and activity dispersion $\sigma_{\log R'_{HK}(T_{\text{eff}})}$ fitted to the data. According to our observations, the general trend indicates that the most active stars ($\log R'_{HK}(T_{\text{eff}}) > -4.7$) are in the saturated regime of activity dispersion. Since this region is not well-sampled by our observations, we preferred to rule out these stars from the fit:

$$\sigma_{\log R'_{HK}(T_{\text{eff}})} = 0.62 + 0.119 \log R'_{HK}(T_{\text{eff}}). \quad (10)$$

For instance, considering the measured solar mean activity level of $\log R'_{HK}(T_{\text{eff}}) = -5.021$, the Eq. 10 predicts $\sigma_{\log R'_{HK}}^{\text{fit}} = 0.023$ which is in agreement with the dispersion measured through cycles 10–24 ($\sigma_{\log R'_{HK}}^{\text{cycles 10-24}} = 0.016$). This result is evidence that the solar variability follows the same trend observed in solar twins. As an example, we applied this equation to the inactive stars shown in Fig. 5. Our predictions are in agreement with the observed activity dispersions within 0.005 dex. This relation will be used on Sec. 3 to estimate the lower limits on chromospheric age dating due to cycle variability and also the role of stellar variability on the scatter observed in the age-activity relation.

In Fig. 6, it is possible to see that young stars tend to show higher dispersion in their activity measurements while the oldest ones exhibit the lowest activity variations. It is worth noting that the robustness of the activity measurements is a balance between the amount of detectable flux excess (after correcting the photospheric signature) and the typical cycle activity modulations. Therefore, younger and older stars tend to show different features in the age-activity diagram. The former shows high levels of activity that can be easily detectable, in contrast with their higher amplitude cycle modulations. In the case of stars with very similar atmospheric parameters, the amplitude of cycle fluctuations can blur minor mass and chemical composition effects on chromospheric indicators. On the other hand, older stars with smaller activity variations and lower flux excess are the most suitable targets to detect these effects on chromospheric indicators. These minor mass and chemical composition effects will be discussed in the next sections.

3. The activity-age relation

3.1. Stellar ages

The isochronal ages of our sample were derived by comparing the observed location of each star in stellar parameter space (T_{eff} , $\log g$, $[\text{Fe}/\text{H}]$, $[\alpha/\text{Fe}]$, and V absolute magnitude) with predictions of stellar evolution theory, as computed by the Yonsei-Yale group (Yi et al. 2001; Kim et al. 2002). Our method is an extension of the procedures adopted in Ramírez et al. (2014) and Tucci Maia et al. (2016), since we included in our analysis other relevant variables that also constrain the morphology of the isochrones such as V magnitude, the trigonometric distance from GAIA DR1 and Hipparcos, and $[\alpha/\text{Fe}]$ information.

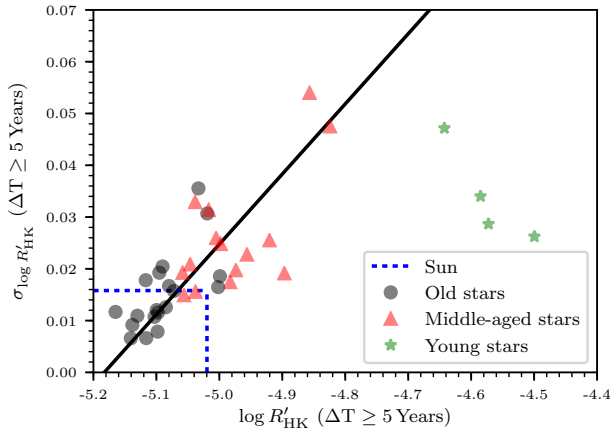


Fig. 6. $\sigma_{\log R'_{\text{HK}}(T_{\text{eff}})}$ vs. $\log R'_{\text{HK}}(T_{\text{eff}})$ relation for stars monitored by more than 5 years. The solid black line is the best fit. Green stars, red triangles, and black circles are solar twins with ages $t \leq 2$ Gyr, $2 < t \leq 6.5$ Gyr, and $t > 6.5$ Gyr, respectively. The blue dashed line stands for solar activity mean and dispersion.

³. This improved isochronal age-dating approach with additional constraints results in narrower age probability distributions and, consequently, more internally consistent age estimates. Details of this straightforward probabilistic approach are given in Spina et al. (2018).

Typically, isochrone ages of main-sequence stars are very uncertain due to poorly-known luminosities, which, in some cases, stems from inaccurate distances/parallaxes, and the fact that stars evolve slowly during that stage. For solar twins, this is not an issue because the stars' precise spectroscopic parameters (T_{eff} , $[\text{Fe}/\text{H}]$, $\log g$, and $[\alpha/\text{Fe}]$) are statically combined with their luminosities. Indeed, the precision of stellar ages for solar twins is as good as, if not better than those obtained for slightly evolved stars, for which the isochrone method works best. Moreover, because the isochrone sets can be slightly modified to match precisely the solar parameters, ages of solar twins can be made not only very precise, but also reasonably accurate (Meléndez et al. 2012, 2014).

In addition, more sophisticated Bayesian approaches to deriving stellar isochronal ages might be necessary to investigate the long-term evolution of heterogeneous populations (see, e.g., Casagrande et al. 2011). On the other hand, as we are analysing a sample of stars with very precise atmospheric parameters, the prior distribution becomes approximately constant within the uncertainties of the atmospheric parameters given by the observations (Pont & Eyer 2004). In other words, the problem converges to the traditional frequentist chi-squared fit. Moreover, Chanamé & Ramírez (2012, their Figure 7) have shown that at least one of these approaches which uses Bayesian techniques results in ages which are only slightly offset from those computed using our simpler approach.

Notice that our differential isochrone method gives an age of $4.2^{+0.3}_{-0.5}$ for 18 Sco, in good agreement with the seismic age of $3.66^{+0.44}_{-0.50}$ Gyr by Li et al. (2012). In addition, for the 16 Cyg pair of solar twins (Ramírez et al. 2011), our method predicts an age of 6.4 ± 0.2 Gyr (Tucci-Maia et al. 2018, submitted) which is also close to its seismic age (average of 7.0 ± 0.1 Gyr) estimated

³ Except for HIP29525 and HIP109110, for which rotational ages were adopted.

by van Saders et al. (2016). Thus, our method seems valid also for stars around the solar age and somewhat older.

3.2. Activity-age relation using the updated $\log R'_{\text{HK}}(T_{\text{eff}})$

After averaging all multiple nightly binned activity observations together with its respective standard deviation and estimating the isochronal ages, we analyse now the age-activity diagram of solar twins. The isochronal age-dating method is not optimized for young main-sequence stars. In this region, the isochrones are clumped next to the *Zero Age Main-Sequence*, mapping regimes of very different evolutionary speeds. These differences are translated by a statistical approach into asymmetric probability age distributions that are tailed towards older age solutions. This means that, for stars around 1 Gyr, it can be only reasonable to constrain an upper limit for the isochronal ages. Therefore, to overcome this limitation and derive a consistent age-activity relation for younger stars, we chose to simplify our approach assigning a typical age and activity level for this class of stars. Nine stars younger than 1 Gyr (excluding the outlier HIP114615⁴) were selected in our sample, being classified for the sake of simplicity as a single cluster with mean activity level of $\log R'_{\text{HK}}(T_{\text{eff}}) = -4.54 \pm 0.09$ and a typical age of $0.60^{+0.19}_{-0.14}$ Gyr which is in good agreement with Hyades' canonical age (Perryman et al. 1998, 0.625 Gyr) and activity level (Mamajek & Hillenbrand 2008, $\log R'_{\text{HK}}(B - V) = -4.50 \pm 0.09$). It is convenient to establish ≈ 0.6 Gyr as our lower limit to young and active stars because, at this age range, according to gyrochronology relations, it is expected the convergence of stellar rotation evolution into well-defined sequence depending only on rotation, age, and mass (or a suitable proxy of it), in a first order approach (Barnes 2007; Barnes & Kim 2010; Mamajek & Hillenbrand 2008).

In Fig. 7 (left panel), we show the age-activity relation of solar twins from 0.6 to 9 Gyr. After an extensive radial-velocity monitoring of the whole sample, dos Santos et al. (2017) detected a considerable fraction of spectroscopic binaries of 25% (21 stars, see Sec. 2.2) and an overall multiplicity fraction (taking into account the wide-binary systems) of $\approx 42\%$. The presence of an unresolved companion in the spectra might bias the determination of atmospheric parameters and, especially, the activity measurements. So, after the RV monitoring, we are confident that our sample of isolated solar twins is suitable for the age-activity (AC) analysis. In the case of wide-binaries, they are visually resolved, showing large orbital separation that prevents the angular momentum transfer between the components, so these targets can be considered as isolated stars. Our age-activity analysis is restricted to a sample of 60 single and wide-binary stars (82 stars – 21 spectroscopic binaries – HIP114615). In addition, the wide-binary star HIP77052 (angular separation of only 4.4") was also discarded since it shows very asymmetric age errorbars, very high level of chromospheric activity for the assigned age, and chemical abundance anomalies reported in Spina et al. (2018). As a result, the final sample used to fit the age-activity relation is composed of 59 solar twins spanning the ages from 0.6 to 9 Gyr. In order to posterior check the solar activity behaviour as a function of the other solar twins of same age, we preferred to not include the Sun as an age-activity calibrator.

Different functional forms were tested to the data and the best solution found was a simple power-law:

$$\log(\text{Age}) = 0.0534 - 1.92 \log R'_{\text{HK}}(T_{\text{eff}}). \quad (11)$$

⁴ This peculiar star was excluded in the analysis because of its very asymmetric age errorbar and low activity level.

The error of the slope coefficient is 0.01 and the fractional fitting error found in age is $\approx 20\%$ ⁵. The estimated chromospheric age of the Sun is 4.9 ± 1.0 Gyr and, for the young cluster of solar twins is 0.63 ± 0.12 Gyr. It is worth noticing that we are avoiding the young and saturated regime (ages < 0.5 Gyr). So our function is valid for intermediate to old stars ($0.6 \lesssim \text{ages} \lesssim 9$ Gyr) and it can be interpreted as an approximation of a more complex activity evolution that also covers the young and activity saturated regime (Mamajek & Hillenbrand 2008).

It is convenient to estimate the effect of the cycle modulations on the age-activity diagram. So, we propagated the errors of Eq. 11:

$$\sigma_{\log(\text{Age})}^{\text{variability}} = 1.92 \sigma_{\log < R'_{\text{HK}} >}. \quad (12)$$

This equation enable us to estimate the lower limit of chromospheric age error due to stellar cycle variability, assuming that all solar twins follow the age-activity trend shown in Fig. 7. The term $\sigma_{\log < R'_{\text{HK}} >}$ corresponds to the stellar variability that could be constrained thanks to the multiple observations of our stars (Eq. 10), yielding:

$$\sigma_{\log(\text{Age})}^{\text{variability}} = 1.19 + 0.23 \log R'_{\text{HK}}(T_{\text{eff}}). \quad (13)$$

The $\sigma_{\log(\text{Age})}^{\text{variability}}$ vs. $\log R'_{\text{HK}}(T_{\text{eff}})$ relation is not well-constrained for stars more active than $\log R'_{\text{HK}}(T_{\text{eff}}) \approx -4.6$. In Fig. 7 (left panel), it is also shown the expected 2σ cycle fluctuations following the Eqs. 11 and 13. Almost all solar twins are scattered around the overall banana-like trend predicted by our age-activity relation, and the amplitude of the observed scatter is in good agreement with the predicted intrinsic cycle variability, for a given age.

In order to verify the statistical significance of the age-activity relation, we calculated the Pearson correlation coefficient (R), setting minimum ages starting at 0 and increasing in steps of 0.1 Gyr until 9 Gyr, as shown in Fig. 7 (right panel). Then, we binned the age steps in wider intervals of 1 Gyr, estimating the mean false alarm probability and its dispersion within each bin. We can see quantitatively that our data do not follow the age-activity trend found by Pace (2013). The false-alarm probability around 2 or 3 Gyr is between $10^{-10}\%$ and $10^{-7}\%$, respectively. For stars older than 6-7 Gyr the correlation becomes so low that the probability of a false alarm is greater than 1%. So, in the light of our data, we can confidently say that the age-activity relation evolves until at least 6-7 Gyr.

On the other hand, no conclusion could be drawn about an *intrinsic lack of activity evolution* after this interval due to poor sampling, age uncertainties and possible influence of other stellar parameters on chromospheric activity levels, for example.

Still, we could go one step further and visually inspect in detail the end of the age-activity diagram isolating the variables that are known to affect the activity levels of the most inactive stars such as mass, metallicity and Ca abundances. Thus, in order to visualize better the pure effect of the age-activity correlation, we restricted our sample to the best old solar twins (age > 4 Gyr) available in our sample within ± 0.05 of the solar values in M/M_{\odot} , $[\text{Fe}/\text{H}]$, and $[\text{Ca}/\text{H}]$ (Spina et al. 2018). In Fig. 8 (upper

⁵ Only two stars in our sample (HIP15527 and HIP44713) show residuals outside the 2σ domain predicted by our AC calibration. To evaluate the impact of these stars on AC calibration, we performed a single round of 2σ -clipping removal and recalibrated the AC relation for the remaining stars. The slope coefficient remained constant (within ± 0.01) resulting in identical chromospheric age distributions yielded by both approaches (within $\approx 2\%$).

left panel), the end of the AC diagram is shown, followed by the predictions of Eq. 11 and 13 for $\log R'_{\text{HK}}(T_{\text{eff}})$ activity index. The upper right panel of Fig. 8 is the same statistical analysis of Fig. 7 (right panel) applied only to the best old solar twins. The same statistical analysis was also repeated for $\log R'_{\text{HK}}(B - V)$ activity index (lower panels) and, albeit with slightly lower statistical significance in comparison to the $\log R'_{\text{HK}}(T_{\text{eff}})$ vs. age analysis, it is still possible to detect the activity evolution until ≈ 6 Gyr.

We confirmed that the AC relation remains statistically relevant after the solar age also for the most homogeneous group of stars. The typical chromospheric age error derived for these stars is $\approx 13\%$ or about 1 Gyr for a typical 7 Gyr old solar twin. Possibly, the poor sampling after ≈ 7 Gyr together with the increasing ratio between isochronal age errors and the dynamical age range (from 7 to 9 Gyr) are responsible for the lack of statistical significance observed after this domain. In Table 3, we show the performance of our age-activity calibration for old stars (age > 1 Gyr) with progressively longer time-span coverage of Ca II observations (from 5 to ~ 13 years). Typically, our calibration yields a chromospheric age error of about 15%, independent on time-span restrictions.

The Sun is a key target to constrain the age-activity relations, therefore it is important to verify whether it has a typical level and dispersion of chromospheric activity in comparison to other stars with similar parameters. It can be seen in Fig. 7 (left panel) and Fig. 8 (left panel) that the Sun is a normal star in comparison to other solar twins, following the overall age-activity trend and also a compatible activity dispersion expected for a typical 4 Gyr old star.

4. Discussion

According to our results, the chromospheric activity index $\log R'_{\text{HK}}(T_{\text{eff}})$ is an interesting clock up to ≈ 7 Gyr. Besides the age evolution, the chromospheric activity is well-known to be also correlated with stellar mass and other atmospheric parameters such as metallicity. In this regard, our analysis using a group of stars with precise and very similar atmospheric parameters enabled us to mitigate these effects, testing the limits of the age-activity relation. Our analysis does not indicate that the age-activity relation flattens out for stars older than 1 to 3 Gyr as, described by Pace & Pasquini (2004) and Pace (2013). Probably, the simplest explanation for the lack of chromospheric evolution in old field stars is the combination of mass/metallicity dependencies that arises from selection effects (Lorenzo-Oliveira et al. 2016b). In addition to mass effects, distant open clusters members also suffer from interstellar contamination of Ca II lines, biasing the activity measurements towards inactive levels (Curtis 2017).

If there is a sudden decrease of the activity level followed by a relatively constant and inactive phase, the Rossby number vs. activity diagram should reveal this behaviour. In this sense, Mamajek & Hillenbrand (2008) did not find any discontinuity in the age-rotation-activity relation for stars with ages $\gtrsim 1$ Gyr. Also, in the light of new open cluster data from the Kepler mission, the gyrochronology relations show very consistent results for solar-type stars from 1 to 4 Gyr old (Meibom et al. 2011, 2015; Barnes et al. 2016b). After ≈ 4 Gyr, the scenario of smooth rotational evolution predicted by previous gyrochronology relations is still under debate. van Saders et al. (2016) combined the rotational periods of intermediate age open clusters members and old field solar-type stars with measured rotational periods (photometric or asteroseismic rotational periods) to point out that, at some threshold Rossby number, a rapid change in the topology of the

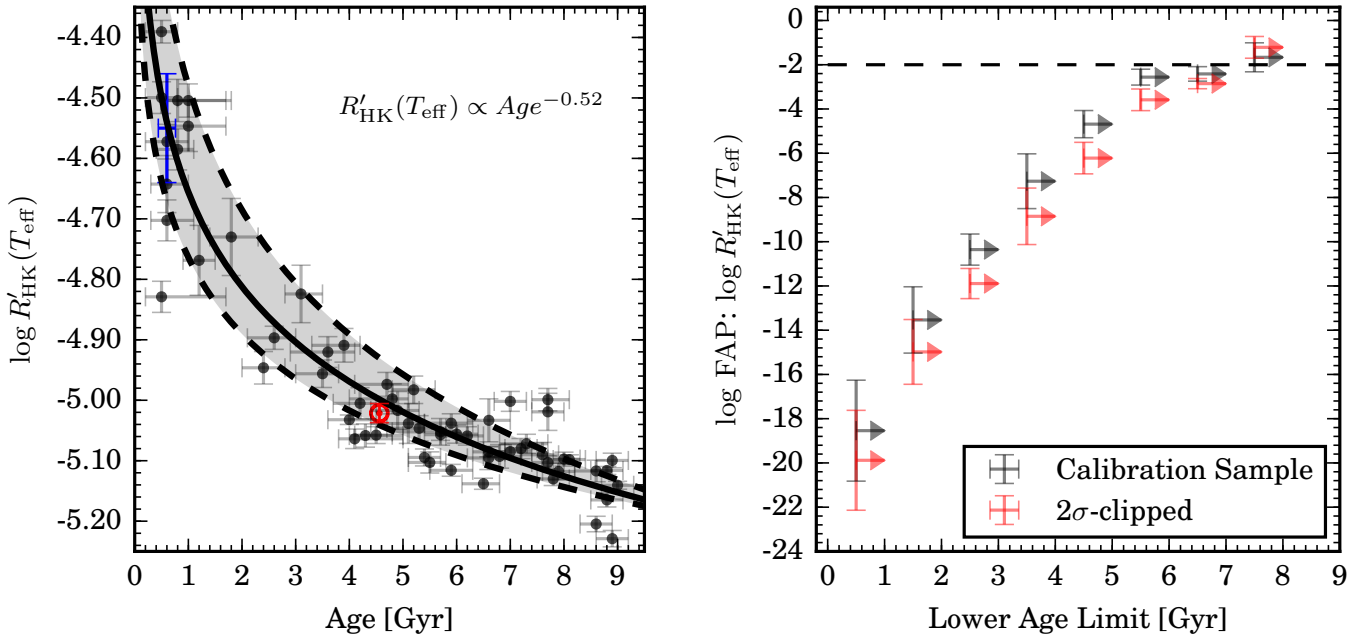


Fig. 7. *Left panel:* Age-Activity relation derived for solar twins. The solid line is the best fit. The Sun is plotted with its usual symbol. Stars younger than 1 Gyr are represented as a single cluster (blue error bar) with mean activity $\log R'_{\text{HK}}(T_{\text{eff}}) = -4.54 \pm 0.09$ and age $= 0.6 \pm 0.2$ Gyr. The shaded region is the 2σ activity variability prediction band. *Right panel:* Statistical significance of the AC relation as a function of the lower age limit. Black and red symbols are the results for the entire calibration sample and after a single round of 2σ -clipping removal, respectively. It can be seen that the false-alarm probabilities reach $\approx 1\%$ around 7 Gyr.

magnetic fields happens inside the star and this effect is translated into an inefficient magnetic braking for relatively old stars. In brief, the observational effect of this change is the overabundance of unexpected old rapid rotators. Therefore, according to their analysis, in the case of solar mass stars, for example, the usual gyrochronology relations become ineffective for ages older than ≈ 4 Gyr.

In contrast, our age-activity diagram does not indicate any sign of discontinuity or overpresence of old and relatively rapid rotators due to an inefficient magnetic braking, assuming that activity and rotational evolutions are coupled. Barnes et al. (2016a) analysed the Kepler sample stars with measured rotational periods and asteroseismic ages and, after removing the metal-poor and post main-sequence stars ($\log g < 4.2$), they found a good agreement between seismic and rotational ages up to 8-9 Gyr. A similar result was previously found by do Nascimento et al. (2014) analysing solar analogs and candidates of solar twins from the Kepler mission. Both results are consistent with our findings in this work.

5. Summary and Conclusions

The main goal of this paper is to revisit the activity-age relation using HARPS high-resolution time-series observations of 82 solar twins whose precise isochronal ages and other important physical parameters (such as T_{eff} , $[\text{Fe}/\text{H}]$, $\log g$ and $[\text{Ca}/\text{H}]$ abundances) have been obtained (Spina et al. 2018; Bedell et al. 2018). To do so, the Ca II H \& K S indices were calculated following Mount Wilson prescriptions presented in Wright et al. (2004) and then, we revisited the MW calibration equations to build a new activity index $\log R'_{\text{HK}}(T_{\text{eff}})$, replacing the color index dependency by T_{eff} (Eqs. 8 and 7). This modification mitigates the metallicity degeneracy present in (B-V) color indices.

The solar S_{MW} were calculated also from HARPS observations and related to sunspot number (Eq. 9). Thus, anchored on the sunspot number time-series from the Royal Observatory of Belgium, we could reconstruct the solar activity level along the cycles 10-24 (1856-2017, $\langle S_{\text{MW}} \rangle (10-24) = 0.1694 \pm 0.0024$, which is in excellent agreement with the Egeland et al. (2017) analysis recalibrating the Sun's activity level. Through multiple observations of solar twins, we detected that younger stars tend to show higher activity dispersion in comparison to older counterparts. Therefore, a simple relation between mean activity level ($\langle R'_{\text{HK}} \rangle$) and long-term activity variation ($\sigma_{\langle R'_{\text{HK}} \rangle}$) could be derived (Eq. 10). The solar long-term activity variation follows the same trend observed for solar twins with similar age and mean activity levels, thus we conclude that the Sun has a mean activity level typical for its age. This relation helped us to predict the scatter due to stellar variability on the age-activity evolution of solar twins.

Interestingly, the age-activity relation found for solar twins follows the Skumanich-like function $\langle R'_{\text{HK}} \rangle \propto \text{Age}^{-0.52}$ (Eq. 11) similar to the power-law derived by Soderblom et al. (1991). The fractional age uncertainty is around 20% and the AC relation is valid only for solar-mass solar-metallicity stars with ages between 0.6 to 9 Gyr. Almost all stars in our sample are placed within the predicted AC variability band for a given age, indicating that, in principle, a significant part of the observed scatter could be explained by long-term cycle modulations. For our sample, tests of statistical significance of the age-activity relation rule out the lack of evolution scenario after ≈ 2 Gyr proposed by Pace & Pasquini (2004) and Pace (2013). So, our approach can be applied to age-date solar twins to at least 6-7 Gyr, where the false-alarm probability reaches $\approx 1\%$. Alternatively, as we consider only the best solar twins available in our sample (solar within ± 0.05 in M/M_{\odot} , $[\text{Fe}/\text{H}]$, and $[\text{Ca}/\text{H}]$), the chromospheric

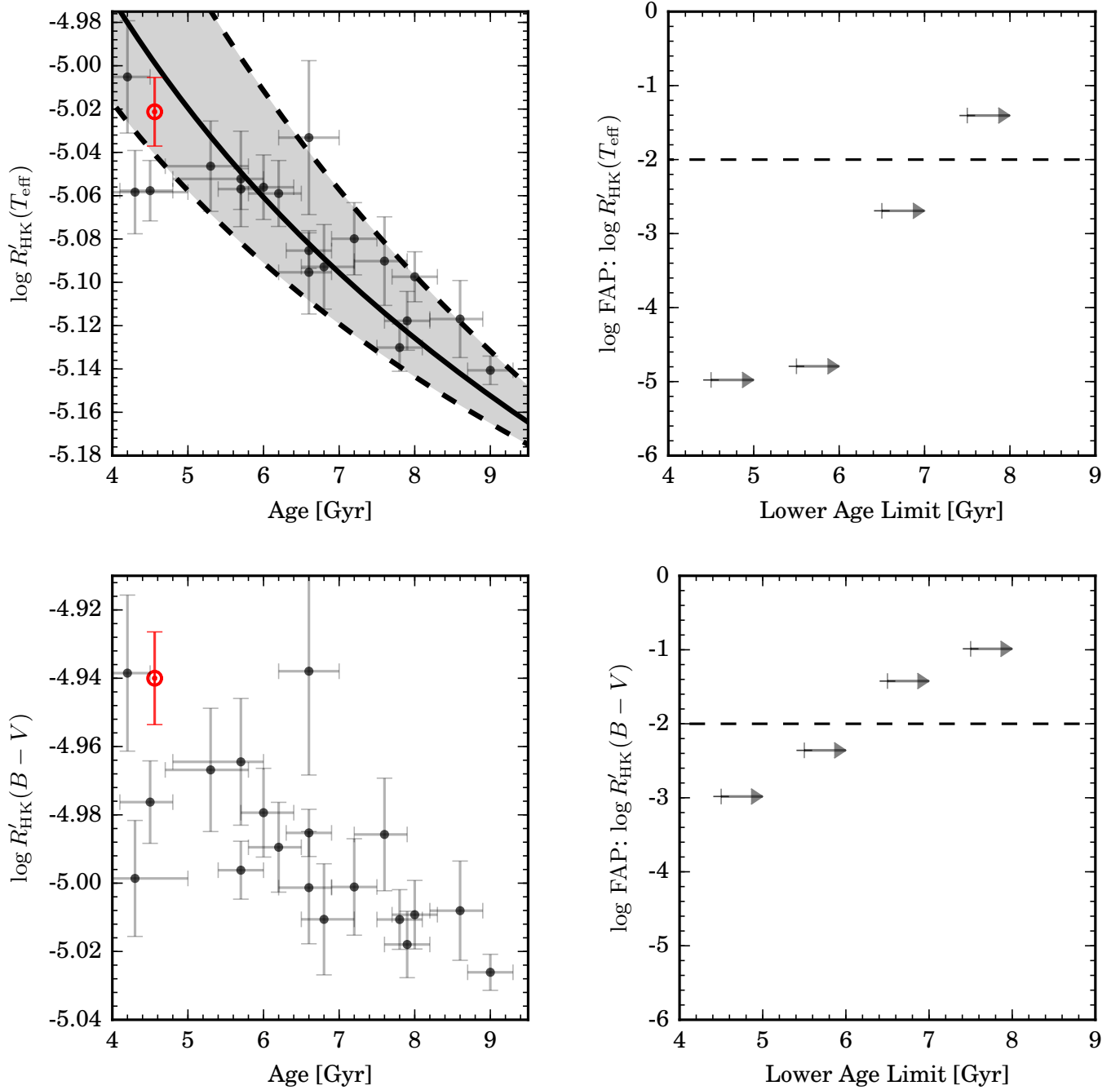


Fig. 8. *Left panels:* End of the age-activity relation of solar twins for $\log R'_{\text{HK}}(T_{\text{eff}})$ (upper panel) and $\log R'_{\text{HK}}(B-V)$ (lower panel). The solid black line is the AC calibration from Eq. 11 and the shaded area represents the 2σ variability prediction band for $\log R'_{\text{HK}}(T_{\text{eff}})$. The Sun is plotted in red as its usual symbol. *Right panels:* Same statistical analysis of Fig. 7 applied to the best old solar twins available in our sample.

activity seems to evolve monotonically towards the end of the main-sequence (≈ 9 Gyr). This result is in line with previous works using open clusters and field stars with precise ages (Mamajek & Hillenbrand 2008; do Nascimento et al. 2014; Barnes et al. 2016a; Lorenzo-Oliveira et al. 2016a), reinforcing the use of chromospheric activity as an age diagnostic over a wide range of ages.

Acknowledgements. We would like to acknowledge the anonymous referee, whose comments have unquestionably led to an improved paper. DLO acknowledges the support from FAPESP (2016/20667-8). JM thanks support from FAPESP (2012/24392-2) and CNPq (Productivity Fellowship).

References

- Airapetian, V. S. & Usmanov, A. V. 2016, *ApJ*, 817, L24
 Baliunas, S. L., Donahue, R. A., Soon, W. H., et al. 1995, *ApJ*, 438, 269
 Barnes, S. A. 2007, *ApJ*, 669, 1167
 Barnes, S. A. & Kim, Y.-C. 2010, *ApJ*, 721, 675
 Barnes, S. A., Spada, F., & Weingrill, J. 2016a, *Astronomische Nachrichten*, 337, 810
 Barnes, S. A., Weingrill, J., Fritzewski, D., Strassmeier, K. G., & Platais, I. 2016b, *ApJ*, 823, 16
 Bedell, M., Bean, J. L., Melendez, J., et al. 2018, *ArXiv e-prints*
 Bedell, M., Meléndez, J., Bean, J. L., et al. 2015, *A&A*, 581, A34
 Bertello, L., Pevtsov, A., Tlatov, A., & Singh, J. 2016, *Sol. Phys.*, 291, 2967
 Booth, R. S., Poppenhaeger, K., Watson, C. A., Silva Aguirre, V., & Wolk, S. J. 2017, *MNRAS*, 471, 1012

- Buccino, A. P. & Mauas, P. J. D. 2008, *A&A*, 483, 903
- Busà, I., Aznar Cuadrado, R., Terranegra, L., Andretta, V., & Gomez, M. T. 2007, *A&A*, 466, 1089
- Carlos, M., Nissen, P. E., & Meléndez, J. 2016, *A&A*, 587, A100
- Casagrande, L., Schönrich, R., Asplund, M., et al. 2011, *A&A*, 530, A138
- Chanamé, J. & Ramírez, I. 2012, *ApJ*, 746, 102
- Curtis, J. L. 2017, *AJ*, 153, 275
- Desidera, S., Gratton, R. G., Lucatello, S., Claudi, R. U., & Dall, T. H. 2006, *A&A*, 454, 553
- Do Nascimento, Jr., J. D., Castro, M., Meléndez, J., et al. 2009, *A&A*, 501, 687
- do Nascimento, Jr., J.-D., García, R. A., Mathur, S., et al. 2014, *ApJ*, 790, L23
- do Nascimento, Jr., J.-D., Vidotto, A. A., Petit, P., et al. 2016, *ApJ*, 820, L15
- dos Santos, L. A., Meléndez, J., Bedell, M., et al. 2017, *ArXiv e-prints*
- dos Santos, L. A., Meléndez, J., do Nascimento, J.-D., et al. 2016, *A&A*, 592, A156
- Duncan, D. K., Vaughan, A. H., Wilson, O. C., et al. 1991, *ApJS*, 76, 383
- Egeland, R., Soon, W., Baliunas, S., et al. 2017, *ApJ*, 835, 25
- Fuhrmann, K., Chini, R., Kaderhandt, L., & Chen, Z. 2017, *ApJ*, 836, 139
- Garcés, A., Catalán, S., & Ribas, I. 2011, *A&A*, 531, A7
- Gray, R. O., Corbally, C. J., Garrison, R. F., et al. 2006, *AJ*, 132, 161
- Henry, T. J., Soderblom, D. R., Donahue, R. A., & Baliunas, S. L. 1996, *AJ*, 111, 439
- Jenkins, J. S., Jones, H. R. A., Tinney, C. G., et al. 2006, *MNRAS*, 372, 163
- Jenkins, J. S., Murgas, F., Rojo, P., et al. 2011, *A&A*, 531, A8
- Karak, B. B., Kitchatinov, L. L., & Choudhuri, A. R. 2014, *ApJ*, 791, 59
- Kim, Y.-C., Demarque, P., Yi, S. K., & Alexander, D. R. 2002, *ApJS*, 143, 499
- Lachaume, R., Dominik, C., Lanz, T., & Habing, H. J. 1999, *A&A*, 348, 897
- Lallement, R., Vergely, J.-L., Valette, B., et al. 2014, *A&A*, 561, A91
- Li, T. D., Bi, S. L., Liu, K., Tian, Z. J., & Shuai, G. Z. 2012, *A&A*, 546, A83
- Lo Curto, G., Pepe, F., Avila, G., et al. 2015, *The Messenger*, 162, 9
- Lorenzo-Oliveira, D., Porto de Mello, G. F., Dutra-Ferreira, L., & Ribas, I. 2016a, *A&A*, 595, A11
- Lorenzo-Oliveira, D., Porto de Mello, G. F., & Schiavon, R. P. 2016b, *A&A*, 594, L3
- Lovis, C., Dumusque, X., Santos, N. C., et al. 2011, *ArXiv e-prints*
- Lyra, W. & Porto de Mello, G. F. 2005, *A&A*, 431, 329
- Mamajek, E. E. & Hillenbrand, L. A. 2008, *ApJ*, 687, 1264
- Mayor, M., Pepe, F., Queloz, D., et al. 2003, *The Messenger*, 114, 20
- Meibom, S., Barnes, S. A., Latham, D. W., et al. 2011, *ApJ*, 733, L9
- Meibom, S., Barnes, S. A., Platais, I., et al. 2015, *Nature*, 517, 589
- Meléndez, J., Asplund, M., Gustafsson, B., & Yong, D. 2009, *ApJ*, 704, L66
- Meléndez, J., Bean, J. L., Bedell, M., et al. 2015, *The Messenger*, 161, 28
- Meléndez, J., Bedell, M., Bean, J. L., et al. 2017, *A&A*, 597, A34
- Meléndez, J., Bergemann, M., Cohen, J. G., et al. 2012, *A&A*, 543, A29
- Meléndez, J., Ramírez, I., Karakas, A. I., et al. 2014, *ApJ*, 791, 14
- Meléndez, J., Shchukina, N. G., Vasiljeva, I. E., & Ramírez, I. 2006, *ApJ*, 642, 1082
- Mittag, M., Schröder, K.-P., Hempelmann, A., González-Pérez, J. N., & Schmitt, J. H. M. M. 2016, *A&A*, 591, A89
- Montes, D., López-Santiago, J., Fernández-Figueroa, M. J., & Gálvez, M. C. 2001, *A&A*, 379, 976
- Ng, Y. K. & Bertelli, G. 1998, *A&A*, 329, 943
- Nissen, P. E. 2015, *A&A*, 579, A52
- Noyes, R. W., Hartmann, L. W., Baliunas, S. L., Duncan, D. K., & Vaughan, A. H. 1984, *ApJ*, 279, 763
- Oranje, B. J. & Zwaan, C. 1985, *A&A*, 147, 265
- Pace, G. 2013, *A&A*, 551, L8
- Pace, G. & Pasquini, L. 2004, *A&A*, 426, 1021
- Parker, E. N. 1970, *ApJ*, 162, 665
- Pasquini, L. & Pallavicini, R. 1991, *A&A*, 251, 199
- Perryman, M. A. C., Brown, A. G. A., Lebreton, Y., et al. 1998, *A&A*, 331, 81
- Pipin, V. V. & Kosovichev, A. G. 2016, *ApJ*, 823, 133
- Pont, F. & Eyer, L. 2004, *MNRAS*, 351, 487
- Porto de Mello, G. F. & da Silva, L. 1997, *ApJ*, 482, L89
- Ramírez, I., Allende Prieto, C., & Lambert, D. L. 2013, *ApJ*, 764, 78
- Ramírez, I., Fish, J. R., Lambert, D. L., & Allende Prieto, C. 2012a, *ApJ*, 756, 46
- Ramírez, I., Meléndez, J., Bean, J., et al. 2014, *A&A*, 572, A48
- Ramírez, I., Meléndez, J., Cornejo, D., Roederer, I. U., & Fish, J. R. 2011, *ApJ*, 740, 76
- Ramírez, I., Michel, R., Sefako, R., et al. 2012b, *ApJ*, 752, 5
- Reiners, A. & Mohanty, S. 2012, *ApJ*, 746, 43
- Ribas, I., Guinan, E. F., Güdel, M., & Audard, M. 2005, *ApJ*, 622, 680
- Rocha-Pinto, H. J. & Maciel, W. J. 1998, *MNRAS*, 298, 332
- Rutten, R. G. M. 1984, *A&A*, 130, 353
- Rutten, R. G. M. & Schrijver, C. J. 1987, *A&A*, 177, 155
- Schirbel, L., Meléndez, J., Karakas, A. I., et al. 2015, *A&A*, 584, A116
- Schlafly, E. F. & Finkbeiner, D. P. 2011, *ApJ*, 737, 103
- Schlegel, D. J., Finkbeiner, D. P., & Davis, M. 1998, *ApJ*, 500, 525
- Schröder, K.-P., Mittag, M., Hempelmann, A., González-Pérez, J. N., & Schmitt, J. H. M. M. 2013, *A&A*, 554, A50
- Skumanich, A. 1972, *ApJ*, 171, 565
- Soderblom, D. R. 2010, *ARA&A*, 48, 581
- Soderblom, D. R., Duncan, D. K., & Johnson, D. R. H. 1991, *ApJ*, 375, 722
- Spina, L., Meléndez, J., Karakas, A. I., et al. 2018, *MNRAS*, 474, 2580
- Spina, L., Meléndez, J., Karakas, A. I., et al. 2016a, *A&A*, 593, A125
- Spina, L., Meléndez, J., & Ramírez, I. 2016b, *A&A*, 585, A152
- Suárez Mascareño, A., Rebolo, R., & González Hernández, J. I. 2016, *A&A*, 595, A12
- Suárez Mascareño, A., Rebolo, R., González Hernández, J. I., & Esposito, M. 2015, *MNRAS*, 452, 2745
- Tucci Maia, M., Ramírez, I., Meléndez, J., et al. 2016, *A&A*, 590, A32
- van Saders, J. L., Ceillier, T., Metcalfe, T. S., et al. 2016, *Nature*, 529, 181
- Wright, J. T., Marcy, G. W., Butler, R. P., & Vogt, S. S. 2004, *ApJS*, 152, 261
- Yi, S., Demarque, P., Kim, Y.-C., et al. 2001, *ApJS*, 136, 417

Table 1. All the solar twins observed by HARPS, their respective programs and S values compiled from the literature.

HIP	ESO programs	S	σ_S	reference
1954	188.C-0265; 072.C-0488; 096.C-0499; 192.C-0852; 091.C-0936; 183.C-0972; 0100.D-0444	0.179	0.007	1; 3
3203	188.C-0265; 0100.D-0444	0.299	0.006	1; 4
4909	188.C-0265; 0100.D-0444	0.297	0.012	1
5301	092.C-0721; 183.C-0972; 090.C-0421; 072.C-0488; 091.C-0034; 0100.D-0444	0.167	0.012	1
6407*	188.C-0265	0.214	0.012	1
7585	188.C-0265; 0100.D-0444	0.176	0.006	1; 4
8507	188.C-0265; 0100.D-0444	0.171	0.008	1; 2
9349	188.C-0265; 0100.D-0444	0.283	0.012	1
10175	188.C-0265; 0100.D-0444	0.209	0.012	1
10303	188.C-0265; 0100.D-0444	0.167	0.006	1; 4
11915	188.C-0265; 092.C-0721; 093.C-0409; 0100.D-0444	0.181	0.012	1
14501*	188.C-0265; 183.C-0972; 072.C-0488; 192.C-0852; 0100.D-0444	0.157	0.006	1; 4
14614	188.C-0265; 076.C-0155; 0100.D-0444	0.168	0.012	1
15527	183.C-0972; 072.C-0488; 192.C-0852; 0100.D-0444	0.177	0.013	1; 3
18844*	188.C-0265	0.167	0.007	1; 3; 5
19911*	188.C-0265	0.253	0.008	1; 4
22263	188.C-0265; 0100.D-0444	0.279	0.014	1; 2; 4; 5; 6
25670	188.C-0265; 097.C-0571; 0100.D-0444	0.168	0.015	1; 2
28066	188.C-0265; 0100.D-0444	0.155	0.006	1; 4; 6
29432	188.C-0265; 185.D-0056; 0100.D-0444	0.168	0.006	1; 4
29525	072.C-0488; 0100.D-0444	0.343	0.012	1
30037*	188.C-0265	0.166	0.008	1; 2; 7
30158	188.C-0265	0.169	0.011	1; 5
30476	183.C-0972; 188.C-0265; 072.C-0488	0.159	0.006	1; 5
30502	188.C-0265; 183.D-0729	0.168	0.006	1; 7
33094	072.C-0488	0.153	0.012	1
34511	188.C-0265	0.166	0.012	1
36512	183.C-0972; 188.C-0265; 072.C-0488; 091.C-0936	0.170	0.006	1; 7
36515	192.C-0224; 0100.D-0444	0.363	0.012	1
38072	188.C-0265	0.305	0.014	1; 2
40133	188.C-0265	0.160	0.006	1; 4
41317	188.C-0265; 183.C-0972; 072.C-0488	0.164	0.006	1; 4; 5; 7
42333	188.C-0265	0.304	0.015	1; 4
43297	188.C-0265	0.256	0.007	1; 4
44713	072.C-0488; 192.C-0852; 196.C-1006	0.185	0.023	1; 3
44935	188.C-0265; 183.D-0729	0.165	0.006	1; 7
44997	183.D-0729; 188.C-0265; 075.C-0332	0.174	0.012	1; 7
49756	183.D-0729; 188.C-0265	0.164	0.006	1; 4
54102*	188.C-0265; 072.C-0488	0.218	0.008	1; 7
54287	183.D-0729; 188.C-0265; 183.C-0972; 072.C-0488	0.192	0.046	1; 5
54582*	183.D-0729; 072.C-0488; 183.C-0972; 188.C-0265	0.155	0.006	1; 4
62039*	188.C-0265; 183.D-0729	0.155	0.006	1; 4
64150*	188.C-0265	0.159	0.006	1; 4; 6
64673	188.C-0265	0.163	0.012	1
64713	188.C-0265; 183.D-0729	0.167	0.006	1; 7
65708*	188.C-0265	0.155	0.006	1; 4
67620*	188.C-0265	0.215	0.008	1; 4; 5
68468	188.C-0265; 097.C-0571	0.156	0.012	1
69645	188.C-0265	0.164	0.012	1
72043*	188.C-0265	0.168	0.006	1; 4
73241*	188.C-0265	0.172	0.014	1; 5
73815	188.C-0265; 075.C-0332	0.161	0.012	1
74389	072.C-0488	0.171	0.012	1
74432	188.C-0265	0.149	0.006	1; 4
76114	188.C-0265	0.161	0.006	1; 4
77052	075.C-0332; 188.C-0265	0.196	0.006	1; 4; 5
77883	188.C-0265; 183.D-0729	0.166	0.006	1; 7
79578*	188.C-0265	0.217	0.006	1; 5
79672	183.D-0729; 185.D-0056; 188.C-0265; 192.C-0852; 183.C-0972; 072.C-0488; 196.C-1006; 077.C-0364; 099.C-0491	0.170	0.006	1; 2; 4; 6; 7
79715	188.C-0265	0.172	0.013	1; 5
81746*	188.C-0265	0.173	0.011	1; 5
83276*	188.C-0265	–	–	–
85042	188.C-0265; 183.C-0972; 192.C-0852; 089.C-0415; 072.C-0488	0.157	0.006	1; 4
87769*	188.C-0265	0.170	0.012	1
89650	188.C-0265; 183.D-0729; 0100.D-0444	0.165	0.006	1; 7
95962	188.C-0265; 183.C-0972; 072.C-0488; 60.A-9036; 077.C-0364; 0100.D-0444	0.161	0.006	1; 4
96160	188.C-0265; 0100.D-0444	0.187	0.012	1
101905	188.C-0265; 183.D-0729; 0100.D-0444; 099.C-0491	0.216	0.019	1; 3; 3; 5
102040	188.C-0265; 183.D-0729; 0100.D-0444	0.170	0.006	1; 4; 6
102152	292.C-5004; 188.C-0265; 183.D-0729; 0100.D-0444	0.161	0.012	1
103983*	188.C-0265	–	–	–
104045	188.C-0265; 097.C-0571; 092.C-0721; 093.C-0409; 0100.D-0444	0.164	0.012	1
105184	188.C-0265; 183.D-0729; 0100.D-0444	0.231	0.022	1; 3; 5
108158	072.C-0488; 183.C-0972; 0100.D-0444	–	–	–
108468	188.C-0265; 072.C-0488; 183.D-0729; 183.C-0972; 091.C-0936; 192.C-0852; 0100.D-0444	0.163	0.012	1
109821	192.C-0852; 072.C-0488; 196.C-1006; 0100.D-0444	0.159	0.012	1
114328	188.C-0265; 0100.D-0444	–	–	–
114615	188.C-0265	0.191	0.012	1
115577	072.C-0488; 188.C-0265; 192.C-0852; 183.C-0972; 183.D-0729; 196.C-1006; 0100.D-0444	0.160	0.006	1; 5
116906*	072.C-0488; 183.C-0972; 192.C-0852	0.163	0.012	1

Table 1. continued.

HIP	ESO programs	S	σ_S	reference
117367	188.C-0265; 0100.D-0444	0.156	0.012	1
118115	188.C-0265; 0100.D-0444	0.16	0.012	1

- 1 Ramírez et al. (2014)
- 2 Jenkins et al. (2011)
- 3 Jenkins et al. (2006)
- 4 Wright et al. (2004)
- 5 Henry et al. (1996)
- 6 Duncan et al. (1991)
- 7 Meléndez et al. (2009)

Table 2. Parameters of all sample solar twins.

HIP	V	(B-V)	T_{eff}	$\log g$	[Fe/H]	S_{MW}	$\log R'_{\text{HK}}(T_{\text{eff}})$	age (Gyr)	N° Obs	time-span (years)
1954	7.275 ± 0.004	0.681 ± 0.007	5720 ± 2	4.460 ± 0.008	-0.090 ± 0.003	0.177 ± 0.004	-5.000 ± 0.025	4.8 ^{+0.3} _{-0.8}	87	14.0
3203	7.030 ± 0.008	0.620 ± 0.015	5868 ± 9	4.540 ± 0.016	-0.050 ± 0.007	0.314 ± 0.013	-4.500 ± 0.027	0.5 ^{+0.3} _{-0.2}	35	6.0
4909	8.512 ± 0.006	0.637 ± 0.024	5861 ± 7	4.50 ± 0.016	0.048 ± 0.006	0.282 ± 0.012	-4.572 ± 0.028	0.6 ^{+0.3} _{-0.4}	34	6.0
5301	8.449 ± 0.012	0.650 ± 0.009	5723 ± 3	4.395 ± 0.011	-0.074 ± 0.003	0.165 ± 0.002	-5.074 ± 0.016	7.3 ^{+0.4} _{-0.8}	10	11.2
6407*	8.624 ± 0.002	0.652 ± 0.015	5775 ± 7	4.505 ± 0.013	-0.058 ± 0.006	0.223 ± 0.004	-4.772 ± 0.015	1.9 ^{+0.7} _{-0.5}	7	1.2
7585	6.764 ± 0.007	0.648 ± 0.008	5822 ± 3	4.445 ± 0.008	0.083 ± 0.003	0.178 ± 0.004	-4.955 ± 0.023	3.5 ^{+0.7} _{-0.5}	81	6.0
8507	8.899 ± 0.004	0.651 ± 0.018	5717 ± 3	4.460 ± 0.011	-0.099 ± 0.003	0.174 ± 0.005	-5.016 ± 0.030	4.9 ^{+0.4} _{-0.5}	44	6.0
9349	7.992 ± 0.017	0.650 ± 0.009	5818 ± 6	4.515 ± 0.011	-0.006 ± 0.005	0.260 ± 0.017	-4.643 ± 0.048	0.6 ^{+0.3} _{-0.3}	33	6.0
10175	8.18 ± 0.016	0.704 ± 0.018	5719 ± 3	4.485 ± 0.010	-0.028 ± 0.002	0.217 ± 0.014	-4.815 ± 0.053	3.1 ^{+0.3} _{-0.4}	52	6.0
10303	7.629 ± 0.013	0.680 ± 0.016	5712 ± 3	4.395 ± 0.010	0.104 ± 0.003	0.160 ± 0.002	-5.115 ± 0.017	5.9 ^{+0.4} _{-0.4}	56	6.0
11915	8.615 ± 0.008	0.649 ± 0.003	5769 ± 4	4.480 ± 0.011	-0.067 ± 0.004	0.187 ± 0.006	-4.923 ± 0.028	3.6 ^{+0.4} _{-0.7}	54	6.0
14501*	6.966 ± 0.007	0.645 ± 0.010	5738 ± 4	4.305 ± 0.012	-0.153 ± 0.003	0.159 ± 0.001	-5.108 ± 0.009	8.8 ^{+0.3} _{-0.3}	76	14.0
14614	7.840 ± 0.010	0.620 ± 0.015	5803 ± 4	4.450 ± 0.013	-0.109 ± 0.004	0.175 ± 0.003	-4.977 ± 0.021	4.7 ^{+0.3} _{-0.6}	35	11.9
15527	7.362 ± 0.004	0.650 ± 0.006	5779 ± 4	4.335 ± 0.011	-0.064 ± 0.003	0.173 ± 0.003	-5.000 ± 0.019	7.7 ^{+0.4} _{-0.3}	80	14.0
18844*	6.739 ± 0.004	0.676 ± 0.002	5734 ± 3	4.365 ± 0.010	0.014 ± 0.003	0.158 ± 0.001	-5.120 ± 0.007	7.0 ^{+0.3} _{-0.4}	16	1.2
19911*	7.500 ± 0.010	0.661 ± 0.015	5761 ± -	-	-	0.264 ± 0.006	-4.651 ± 0.016	-	7	1.2
22263	5.497 ± 0.012	0.632 ± 0.006	5870 ± 7	4.535 ± 0.013	0.037 ± 0.006	0.276 ± 0.014	-4.585 ± 0.034	0.8 ^{+0.3} _{-0.3}	137	6.0
25670	8.275 ± 0.021	0.659 ± 0.015	5760 ± 3	4.420 ± 0.010	0.054 ± 0.003	0.168 ± 0.005	-5.038 ± 0.033	5.1 ^{+0.3} _{-0.7}	59	6.0
28066	6.592 ± 0.008	0.649 ± 0.010	5742 ± 4	4.300 ± 0.011	-0.147 ± 0.003	0.158 ± 0.001	-5.116 ± 0.007	8.8 ^{+0.7} _{-0.3}	84	6.0
29432	6.861 ± 0.008	0.633 ± 0.007	5762 ± 3	4.450 ± 0.010	-0.112 ± 0.003	0.177 ± 0.004	-4.983 ± 0.024	5.2 ^{+0.4} _{-0.3}	95	6.8
29525	6.442 ± 0.014	0.660 ± 0.005	5741 ± 9	4.520 ± 0.016	-0.012 ± 0.007	0.335 ± 0.016	-4.501 ± 0.031	0.8 ^{+0.3} _{-0.3}	5	12.7
30037*	9.162 ± 0.015	0.682 ± 0.023	5666 ± 3	4.420 ± 0.011	0.007 ± 0.003	0.171 ± 0.006	-5.053 ± 0.037	6.7 ^{+0.3} _{-0.3}	10	5.2
30158	8.479 ± 0.013	0.746 ± 0.020	5678 ± 4	4.365 ± 0.011	-0.004 ± 0.003	0.161 ± 0.002	-5.118 ± 0.014	7.9 ^{+0.3} _{-0.3}	36	5.0
30476	6.671 ± 0.004	0.675 ± 0.040	5709 ± 4	4.280 ± 0.011	-0.033 ± 0.003	0.157 ± 0.001	-5.141 ± 0.007	9.0 ^{+0.3} _{-0.3}	110	13.3
30502	8.667 ± 0.015	0.664 ± 0.016	5731 ± 4	4.400 ± 0.013	-0.057 ± 0.004	0.163 ± 0.002	-5.085 ± 0.013	7.0 ^{+0.4} _{-0.3}	36	7.8
33094	6.038 ± 0.003	0.712 ± 0.005	5629 ± 7	4.110 ± 0.016	0.023 ± 0.005	0.150 ± 0.001	-5.229 ± 0.014	8.9 ^{+0.3} _{-0.3}	88	5.0
34511	7.992 ± 0.010	0.630 ± 0.011	5812 ± 4	4.445 ± 0.012	-0.091 ± 0.003	0.165 ± 0.001	-5.032 ± 0.008	4.0 ^{+0.3} _{-0.5}	29	5.0
36512	7.729 ± 0.011	0.656 ± 0.011	5744 ± 2	4.445 ± 0.008	-0.126 ± 0.002	0.169 ± 0.002	-5.038 ± 0.016	5.9 ^{+0.4} _{-0.5}	65	13.2
36515	6.657 ± 0.004	0.641 ± 0.006	5855 ± 12	4.555 ± 0.023	-0.029 ± 0.009	0.360 ± 0.019	-4.420 ± 0.031	0.5 ^{+0.3} _{-0.3}	46	3.7
38072	9.222 ± 0.002	0.648 ± 0.017	5860 ± 9	4.505 ± 0.018	0.085 ± 0.007	0.313 ± 0.013	-4.504 ± 0.028	1.0 ^{+0.8} _{-0.3}	24	5.0
40133	7.360 ± 0.012	0.660 ± 0.007	5745 ± 3	4.365 ± 0.009	0.116 ± 0.002	0.161 ± 0.002	-5.095 ± 0.014	5.4 ^{+0.3} _{-0.3}	33	5.0
41317	7.807 ± 0.004	0.668 ± 0.027	5706 ± 3	4.385 ± 0.010	-0.081 ± 0.003	0.162 ± 0.001	-5.103 ± 0.011	7.7 ^{+0.3} _{-0.3}	64	13.2
42333	6.738 ± 0.008	0.655 ± 0.005	5846 ± 8	4.500 ± 0.016	0.132 ± 0.006	0.295 ± 0.018	-4.547 ± 0.042	1.0 ^{+0.7} _{-0.4}	37	5.0
43297	7.440 ± 0.008	0.689 ± 0.010	5705 ± 4	4.505 ± 0.009	0.082 ± 0.003	0.243 ± 0.022	-4.730 ± 0.064	1.8 ^{+0.4} _{-0.5}	33	5.0
44713	7.306 ± 0.006	0.668 ± 0.004	5759 ± 3	4.280 ± 0.010	0.063 ± 0.004	0.171 ± 0.005	-5.019 ± 0.031	7.7 ^{+0.3} _{-0.4}	93	12.5
44935	8.739 ± 0.014	0.645 ± 0.022	5771 ± 4	4.370 ± 0.012	0.038 ± 0.004	0.159 ± 0.003	-5.095 ± 0.019	6.6 ^{+0.3} _{-0.4}	30	7.8
44997	8.347 ± 0.023	0.659 ± 0.013	5728 ± 3	4.410 ± 0.011	-0.012 ± 0.003	0.171 ± 0.006	-5.033 ± 0.036	6.6 ^{+0.4} _{-0.4}	33	11.8
49756	7.540 ± 0.008	0.647 ± 0.003	5789 ± 3	4.435 ± 0.009	0.023 ± 0.003	0.163 ± 0.002	-5.058 ± 0.014	4.5 ^{+0.3} _{-0.3}	42	5.0
54102*	8.653 ± 0.004	0.649 ± 0.018	5845 ± 6	4.510 ± 0.010	0.011 ± 0.005	0.228 ± 0.009	-4.728 ± 0.029	0.7 ^{+0.4} _{-0.4}	26	11.0
54287	7.223 ± 0.008	0.680 ± 0.002	5714 ± 4	4.340 ± 0.012	0.107 ± 0.004	0.157 ± 0.001	-5.138 ± 0.009	6.5 ^{+0.3} _{-0.3}	74	13.2
54582*	6.808 ± 0.008	0.613 ± 0.002	5883 ± 5	4.280 ± 0.014	-0.096 ± 0.004	0.158 ± 0.001	-5.056 ± 0.008	6.9 ^{+0.3} _{-0.3}	112	13.1
62039*	7.817 ± 0.009	0.660 ± 0.004	5742 ± 3	4.340 ± 0.010	0.104 ± 0.003	0.157 ± 0.002	-5.124 ± 0.012	6.2 ^{+0.3} _{-0.4}	41	5.0
64150*	6.822 ± 0.061	0.676 ± 0.020	5747 ± 2	4.370 ± 0.008	0.049 ± 0.003	0.160 ± 0.001	-5.100 ± 0.005	6.4 ^{+0.3} _{-0.3}	75	5.0
64673	8.336 ± 0.010	0.640 ± 0.012	5912 ± 5	4.290 ± 0.014	-0.017 ± 0.004	0.163 ± 0.003	-5.007 ± 0.018	6.0 ^{+0.3} _{-0.4}	39	5.0
64713	9.260 ± 0.022	0.649 ± 0.029	5788 ± 4	4.435 ± 0.013	-0.043 ± 0.003	0.165 ± 0.004	-5.046 ± 0.027	5.3 ^{+0.5} _{-0.4}	26	7.8
65708*	7.426 ± 0.008	0.647 ± 0.011	5746 ± 5	4.220 ± 0.012	-0.063 ± 0.005	0.155 ± 0.001	-5.137 ± 0.005	9.0 ^{+0.6} _{-0.3}	10	1.1
67620*	6.430 ± -	0.701 ± 0.050	5660 ± -	-	-	0.220 ± 0.006	-4.823 ± 0.023	7.7 ^{+0.6} _{-0.9}	24	1.1
68468	9.366 ± 0.025	0.654 ± 0.031	5845 ± 5	4.330 ± 0.013	0.071 ± 0.004	0.154 ± 0.003	-5.103 ± 0.021	5.5 ^{+0.3} _{-0.3}	41	5.0
69645	9.416 ± 0.014	0.665 ± 0.004	5751 ± 3	4.435 ± 0.010	-0.026 ± 0.004	0.166 ± 0.003	-5.052 ± 0.022	5.7 ^{+0.4} _{-0.9}	23	5.0
72043*	7.511 ± 0.008	0.636 ± 0.010	5845 ± 4	4.340 ± 0.011	-0.026 ± 0.003	0.178 ± 0.004	-4.942 ± 0.020	6.2 ^{+0.4} _{-0.4}	31	5.0
73241*	6.344 ± 0.008	0.71 ± 0.002	5661 ± 5	4.215 ± 0.014	0.092 ± 0.005	0.175 ± 0.006	-5.032 ± 0.037	8.9 ^{+0.3} _{-0.3}	43	1.1
73815	8.174 ± 0.003	0.663 ± 0.005	5790 ± 3	4.325 ± 0.008	0.023 ± 0.003	0.160 ± 0.002	-5.080 ± 0.017	7.2 ^{+0.3} _{-0.3}	38	11.8
74389	7.773 ± 0.014	0.636 ± 0.012	5845 ± 3	4.440 ± 0.011	0.083 ± 0.003	0.184 ± 0.005	-4.909 ± 0.028	3.9 ^{+0.3} _{-0.3}	31	2.9
74432	6.644 ± 0.008	0.682 ± -	5679 ± 5	4.170 ± 0.013	0.048 ± 0.005	0.150 ± 0.01	-5.205 ± 0.059	8.6 ^{+0.6} _{-0.3}	59	4.8
76114	7.217 ± 0.008	0.656 ± 0.007	5740 ± 3	4.410 ± 0.010	-0.024 ± 0.003	0.162 ± 0.001	-5.084 ± 0.008	6.6 ^{+0.3} _{-0.4}	33	4.8
77052	5.868 ± 0.011	0.686 ± 0.002	5687 ± 3	4.450 ± 0.012	0.051 ± 0.003	0.211 ± 0.016	-4.848 ± 0.060	4.5 ^{+1.1} _{-0.4}	152	11.8
77883	8.755 ± 0.020	0.687 ± 0.024	5699 ± 3	4.375 ± 0.011	0.017 ± 0.003	0.164 ± 0.003	-5.090 ± 0.020	7.6 ^{+0.4} _{-0.4}	32	7.8
79578*	6.533 ± 0.033	0.647 ± 0.006	5810 ± 3	4.465 ± 0.010	0.048 ± 0.003	0.202 ± 0.008	-4.839 ± 0.035	2.4 ^{+0.6} _{-0.4}	48	4.8
79672	5.510 ± 0.009	0.650 ± 0.009	5808 ± 3	4.440 ± 0.009	0.041 ± 0.003	0.170 ± 0.004	-5.005 ± 0.026	4.2 ^{+0.4} _{-0.5}	3775	13.2
79715	8.357 ± 0.014	0.653 ± 0.019	5816 ± 4	4.380 ± 0.011	-0.037 ± 0.004	0.161 ± 0.002	-5.059 ± 0.015	6.2 ^{+0.3} _{-0.3}	34	4.8
81746*	7.024 ± 0.008	0.653 ± -	5715 ± 3	4.370 ± 0.010	-0.091 ± 0.003	0.160 ± 0.001	-5.108 ± 0.008	8.1 ^{+0.3} _{-0.3}	14	4.8
83276*	7.107 ± 0.004	-	5886 ± 6	4.240 ± 0.015	-0.093 ± 0.005	0.155 ± 0.001	-5.078 ± 0.009	7.4 ^{+0.3} _{-0.3}	6	0.3
85042	6.287 ± 0.004	0.679 ± 0.001	5685 ± 3	4.350 ± 0.010	0.030 ± 0.003	0.159 ± 0.001	-5.130 ± 0.011	7.8 ^{+0.3} _{-0.3}	188	10.9
87769*	8.435 ± 0.010	0.685 ± 0.014	5828 ± 3	4.40 ± 0.010	0.072 ± 0.004	0.167 ± 0.004	-5.016 ± 0.024	5.0 ^{+0.3} _{-1.0}	27	4.2
89650	8.944 ± 0.001	0.643 ± 0.022	5851 ± 3	4.415 ± 0.011	-0.015 ± 0.003	0.159 ± 0.003	-5.058 ± 0.022	4.3 ^{+0.7} _{-0.4}	24	8.4
95962	7.265 ± 0.008	0.643 ± 0.015	5805 ± 3	4.380 ± 0.009	0.029 ± 0.003	0.162 ± 0.002	-5.056 ± 0.015	6.0 ^{+0.4} _{-0.4}	78	12.2
96160	8.685 ± 0.013	0.653 ± 0.016	5798 ± 4	4.480 ± 0.012	-0.036 ± 0.003	0.190 ± 0.004	-4.899 ± 0.019	2.6 ^{+0.3} _{-0.5}	40	6.0
101905	7.328 ± 0.008	0.626 ± 0.002	5906 ± 5	4.500 ± 0.011	0.088 ± 0.004	0.211 ± 0.015	-4.769 ± 0.057	1.2 ^{+0.3} _{-0.3}	53	6.0
102040	6.425 ± 0.004	0.613 ± 0.009	5853 ± 4	4.480 ± 0.012	-0.080 ± 0.003	0.176 ± 0.004	-4.950 ± 0.025	2.4 ^{+0.4} _{-0.4}	97	5.5
102152	9.208 ± 0.015	0.669 ± 0.030	5718 ± 4	4.325 ± 0.011	-0.016 ± 0.003	0.159 ± 0.002	-5.118 ± 0.018	8.6 ^{+0.3} _{-0.4}	50	8.4
103983*	8.390 ± -	-	5755 ± -	-	-	0.190 ± 0.007	-4.917 ± 0.039	-	5	3.8
104045	8.336 ± 0.014	0.639 ± 0.004	5826 ± 3	4.410 ± 0.010	0.051 ± 0.003	0.160 ± 0.003	-5.066 ± 0.018	4.1 ^{+0.9} _{-0.3}	35	6.0
105184	6.752 ± 0.004	0.640 ± 0.001	5843 ± 6	4.510 ± 0.011	0.003 ± 0.004	0.237 ± 0.011	-4.702 ± 0.035	0.6 ^{+0.3} _{-0.3}	103	

Table 2. continued.

HIP	V	(B-V)	T_{eff}	$\log g$	[Fe/H]	S_{MW}	$\log R'_{\text{HK}}(T_{\text{eff}})$	age (Gyr)	N° Obs	time-span (years)
115577	7.584 ± 0.008	0.692 ± 0.001	5694 ± 4	4.260 ± 0.010	0.013 ± 0.003	0.154 ± 0.001	-5.165 ± 0.012	$8.8^{+0.3}_{-0.3}$	131	14.0
116906*	7.682 ± 0.009	0.648 ± 0.002	5790 ± 3	4.370 ± 0.009	-0.005 ± 0.003	0.161 ± 0.002	-5.075 ± 0.011	$6.7^{+0.3}_{-0.3}$	26	9.4
117367	7.676 ± 0.009	0.622 ± 0.007	5867 ± 3	4.350 ± 0.010	0.024 ± 0.003	0.159 ± 0.001	-5.056 ± 0.009	$5.7^{+0.3}_{-0.3}$	43	6.0
118115	7.889 ± 0.013	0.633 ± 0.002	5798 ± 4	4.275 ± 0.011	-0.036 ± 0.003	0.157 ± 0.002	-5.099 ± 0.012	$8.0^{+0.3}_{-0.3}$	47	6.0

* Spectroscopic binary

Table 3. Chromospheric age errors as a function of time-span coverage. The age-activity outliers HIP15527 and HIP44713 were removed from this analysis.

Minimum Time-span (yr)	$\langle \text{Age}_{\text{HK}} - \text{Age}_{\text{ISO}} \rangle$ (Gyr)	$\langle (\text{Age}_{\text{HK}} - \text{Age}_{\text{ISO}}) / \text{Age}_{\text{ISO}} \rangle$ –	Number of Stars	$\text{Age}_{\text{ISO}}^{\text{min}}$ (Gyr)	$\text{Age}_{\text{ISO}}^{\text{max}}$ (Gyr)
≥ 5	-0.4 ± 0.9	$16 \pm 6 \%$	33	2.6	9.0
≥ 7	-0.4 ± 1.0	$15 \pm 4 \%$	23	4.2	9.0
≥ 10	-0.5 ± 1.0	$16 \pm 4 \%$	14	4.2	9.0
≥ 13	$+0.0 \pm 0.9$	$13 \pm 3 \%$	6	4.8	9.0